Petroleum Science 21 (2024) 974–986

Contents lists available at ScienceDirect

Petroleum Science

journal homepage: www.keaipublishing.com/en/journals/petroleum-science

Original Paper

Experimental investigation on using CO_2/H_2O emulsion with high water cut in enhanced oil recovery

Xi-Dao Wu [a, b, 1], Peng Xiao [a, 1], Bei Liu [a, *], Guang-Jin Chen [a, **], Jian-Hua Pang [b]

[a] State Key Laboratory of Heavy Oil Processing, China University of Petroleum, Beijing, 102249, China
[b] Ocean Intelligence Technology Center, Shenzhen Institute of Guangdong Ocean University, Shenzhen, 518120, Guangdong, China

ARTICLE INFO

Article history:
Received 12 June 2023
Received in revised form
23 October 2023
Accepted 30 October 2023
Available online 31 October 2023

Edited by Yan-Hua Sun

Keywords:
CO_2/H_2O emulsion
High water cut
CO_2 mobility control
Enhanced oil recovery

ABSTRACT

CO_2 emulsions used for EOR have received a lot of interest because of its good performance on CO_2 mobility reduction. However, most of them have been focusing on the high quality CO_2 emulsion (high CO_2 fraction), while CO_2 emulsion with high water cut has been rarely researched. In this paper, we carried out a comprehensive experimental study of using high water cut CO_2/H_2O emulsion for enhancing oil recovery. Firstly, a nonionic surfactant, alkyl glycosides (APG), was selected to stabilize CO_2/H_2O emulsion, and the corresponding morphology and stability were evaluated with a transparent PVT cell. Subsequently, plugging capacity and apparent viscosity of CO_2/H_2O emulsion were measured systematically by a sand pack displacement apparatus connected with a 1.95-m long capillary tube. Furthermore, a high water cut (40 vol%) CO_2/H_2O emulsion was selected for flooding experiments in a long sand pack and a core sample, and the oil recovery, the rate of oil recovery, and the pressure gradients were analyzed. The results indicated that APG had a good performance on emulsifying and stabilizing CO_2 emulsion. An inversion from H_2O/CO_2 emulsion to CO_2/H_2O emulsion with the increase in water cut was confirmed. CO_2/H_2O emulsions with lower water cuts presented higher apparent viscosity, while the optimal plugging capacity of CO_2/H_2O emulsion occurred at a certain water cut. Eventually, the displacement using CO_2/H_2O emulsion provided 18.98% and 13.36% additional oil recovery than that using pure CO_2 in long sand pack and core tests, respectively. This work may provide guidelines for EOR using CO_2 emulsions with high water cut.

1. Introduction

CO_2 flooding is considered to be an extremely effective method in enhanced oil recovery (EOR) and has been widely applied in the petroleum industry for over 40 years. The injection of CO_2 into reservoirs shows an advancement of oil recovery because of the volume expansion and viscosity decrease of crude oil (Orr and Taber, 1984). Additionally, CO_2 is miscible with crude oil when the pressure exceeds the minimum miscibility pressure, this can lead to remarkable enhancement of oil recovery (Almobarak et al., 2021; Moortgat et al., 2013). Furthermore, the injection of CO_2 into the reservoir may mitigate the greenhouse effect (Ampomah et al., 2016; Li et al., 2016).

However, CO_2 flooding suffers a poor sweep efficiency resulted from the uncontrollable mobility of CO_2, which is accompanied by the phenomenon of gravity override and viscous fingering (Song et al., 2018). Therefore, CO_2 can not contact most of the residual oil in the lower permeability regions (Aryana and Kovscek, 2012). Moreover, the heterogeneity of oil reservoir would aggravate this problem. Some methods such as water alternating gas (WAG) (Afzali et al., 2018), CO_2 thickening and CO_2 foam injection (Burrows et al., 2022; Massarweh and Abushaikha, 2021; Zhang et al., 2019c) have been proposed to control the CO_2 mobility. WAG injection combines the advantages of both CO_2 injection and waterflooding. In the WAG process, the CO_2 dissolved in oil improves the mobility of oil and water slugs provide the stable water–CO_2 for the migration of miscible oil–CO_2 slugs (Massarweh and Abushaikha, 2021). Nonetheless, WAG has a very limited capacity on CO_2 mobility control and does not restrain the gravity segregation arisen from density difference of reservoir fluids. CO_2

* Corresponding author.
** Corresponding author.
E-mail addresses: liub@cup.edu.cn (B. Liu), gjchen@cup.edu.cn (G.-J. Chen).
[1] Xi-Dao Wu and Peng Xiao contribute equally to this work.

https://doi.org/10.1016/j.petsci.2023.10.025

thickening can increase the apparent viscosity of CO_2 markedly and then improves the sweep efficiency, but the poor solubility of thickeners limits the effect on oil recovery (Al Hinai et al., 2019). CO_2 foam is a prospective technology for CO_2 mobility control (Li et al., 2010), and it can reduce CO_2 mobility and stabilize the displacement front during displacement process. Moreover, the high flow resistance arisen from Jamin effect drives CO_2 foam from high-permeability zones to flow into low-permeability zones, which improves sweep efficiency (Zhang et al., 2015).

Because of the high CO_2 density at reservoir conditions (high pressure), it is more appropriate to call the CO_2 foam as CO_2 emulsion. CO_2 emulsion is a CO_2–water dispersion in which the CO_2 phase are separated by lamellae of water phase (Andrianov et al., 2011; Binks et al., 2015). The forming of lamellae impedes CO_2 flowing, which effectively increases CO_2 viscosity and decreases CO_2 relative permeability (Fyen et al., 2020). Further, the increased CO_2 viscosity is caused by viscous shear when lamella move along pore walls and through pore throats, and the reduction in CO_2 permeability is caused by the trapped CO_2 saturation (Song et al., 2020). Although CO_2 emulsion shows a good CO_2 mobility control, the poor stability become the critical shortcoming to restrict the performance of CO_2 emulsion in EOR (Enick et al., 2012). Additionally, the CO_2 emulsion stability could be seriously affected by many factors including crude oil, high temperature, high salinity in the oil reservoir (Alvarenga et al., 2022; Beheshti et al., 2022; Li and Zeng, 2022).

In consideration of the thermodynamical instability of CO_2 emulsion, surfactants are indispensable to reduce the energy required for overcoming Laplace pressure, so as to increase the stability (Rondón-González et al., 2008). Therefore, it is crucial to find a surfactant that can emulsify CO_2 emulsion and stabilize it well (Zhang et al., 2019a). In addition, the performance of reducing CO_2 mobility and increasing apparent viscosity are strongly depended on CO_2 emulsion quality (Safran and Kok, 2022). In general, CO_2 emulsion could be formed with a wide variety of surfactants. Studies have confirmed that cationic surfactant, anionic surfactant, and nonionic surfactant can all be used to stabilize CO_2 emulsion (Da et al., 2018). Recent research has indicated that ionic liquids also show good performances for emulsion production (Kharazi and Saien, 2022; Kharazi et al., 2023). Owing to the advantages of good emulsification ability, wide source, thermal stability and low cost, the nonionic surfactant is a good candidate to stabilize CO_2 emulsion in EOR (Boeije and Rossen, 2018). Adkin et al. confirmed that over twenty nonionic hydrocarbon surfactants expressed the ability of CO_2 emulsion stabilization by decreasing the interfacial tension between CO_2 and H_2O (Adkins et al., 2010). Some nonionic surfactants have been used to generate stable CO_2 emulsion in the presence of crude oil, and the results showed that strong CO_2 emulsion can form in either bulk-foam test or foam-flow test (Jian et al., 2020). Alkyl glucosides (APG) as a nonionic surfactant, has gained considerable interest since they are biodegradable, low toxicity, low cost, and produced from natural (Waltermo et al., 1996). It has been applied in preparing CO_2/H_2O emulsion, and the morphology and stability of the emulsion has been investigated at 11.0 °C and 5.2 MPa (Qin et al., 2018). Our previous study suggested that the CO_2/H_2O emulsion stabilized with APG produced incremental oil recoveries in slim-tube flooding experiments, and the minimum miscible pressure between crude oil and CO_2 was decreased (Wu et al., 2020).

In CO_2 emulsion injection, CO_2 mobility is reduced by the CO_2 bubble trapping and the CO_2 effective viscosity improvement (Grassia, 2015), which mitigates the effect of reservoir heterogeneity on displacement efficiency (Mathew et al., 2018). The flow behavior of CO_2 emulsion in porous media is strongly influenced by factors such as bubble quality, apparent viscosity and texture (Hematpur et al., 2018). Bubble quality referring to gas volume fraction in emulsion and bubble texture referring to the average bubble size must be controlled during the displacement process (Ahmed et al., 2017b). Also, the apparent viscosity of CO_2 emulsion is significantly affected by bubble quality and bubble texture (Osei-Bonsu et al., 2015). Ahmed et al. suggested that the apparent viscosity of CO_2 emulsion increased with the increase in bubble quality and the maximum value was obtained at 85% bubble quality (Ahmed et al., 2017a). Furthermore, studies have confirmed that CO_2 emulsion usually presents shear thinning behavior during the measurement of apparent viscosity (Song et al., 2022). However, the majority of these studies focused on rheology behavior of high quality bubble (high CO_2 fraction) (Yu and Kanj, 2022), and little of them concerned the rheology behavior of CO_2 emulsion with high water cut. Consequently, the work about CO_2 emulsion with high water cut needs to be implemented in view of the requirement of reducing CO_2 consumption because of its price in China. Moreover, when the CO_2 emulsion was used in enhancing oil recovery, these subjects have always been highlighted frequently including emulsification ability, stability of emulsion, CO_2 mobility reduction and oil recovery increment (Abdelgawad et al., 2022). Whereas, most of previous works have only focused on a part or several parts of them.

In this study, the CO_2 emulsion stabilized with APG for CO_2 mobility reduction and enhancing oil recovery is investigated comprehensively. The flooding experiments without oil in sand pack and capillary tube are carried out to evaluate the mobility control efficiency and to measure the apparent viscosity of CO_2/H_2O emulsion. CO_2/H_2O emulsion prepared with 1.5% APG and 40 vol% water cut is used for oil flooding experiments. Both displacement experiments conducted on long sand packs and cores are carried out to confirm enhancing performance of oil recovery with CO_2/H_2O emulsion injection. The results can be useful for understanding the rheological properties and the displacement mechanisms with CO_2/H_2O emulsion. Moreover, the investigation can provide guidelines for the deployment of high water cut CO_2 emulsion to enhance CO_2 flooding process.

2. Experimental methods

2.1. Materials

CO_2 with 99.9% purity was obtained from the Beijing Beifen Gas Industry Corporation. The surfactant alkyl polyglucoside (APG) was provided by the Yiqun Chemical Corporation (China). NaCl, $CaCl_2$, and $MgCl_2$ with analytical reagent grade were purchased from Aladdin Industrial. Brine was made from deionized water with NaCl, $CaCl_2$, and $MgCl_2$, and the total concentration of electrolyte was 15,000 mg/L. Crude oil Ma 18 was provided by Research Institute of Petroleum Exploration and Development, PetroChina. The surfactant solutions were prepared by dissolving surfactant into deionized water and the concentration of surfactant was calculated based on the water mass. All the materials were used as received.

2.2. Morphology and stability evaluation for CO_2/H_2O emulsion

A schematic of the apparatus is shown in Fig. 1. A PVT cell with electromagnetic stirring and piston was used for preparation and observation for CO_2 emulsions. A ISCO pump was used to inject fluid under constant velocity or constant pressure. A manual pump was used to regulate the pressure in the PVT cell through driving the piston inside the cell. The system temperature was regulated by an incubator with a temperature controller.

Aqueous surfactant solutions were prepared by dispersing a

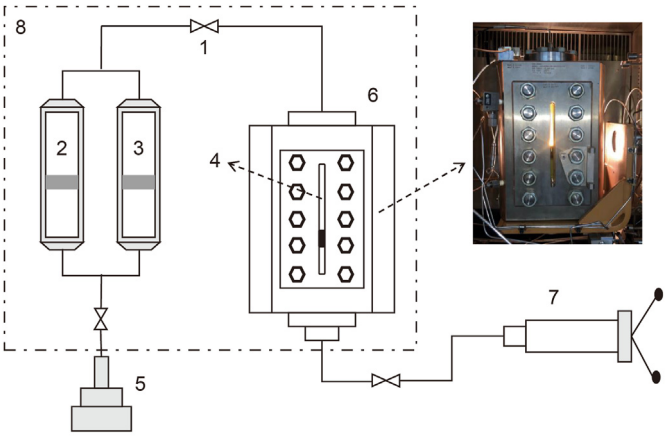

Fig. 1. Schematic diagram of the transparent PVT cell for emulsion evaluation.

certain amount of APG in deionized water. The concentration of surfactant refers to the mass ratio of it to water. A certain volume of surfactant solution and liquid CO_2 were diverted successively into the PVT cell from intermediate containers at constant pressure of 10 MPa. The volumes of two fluids were determined according to the reading of the ISCO pump, and the water cut was calculated by the volume fraction of water in the PVT cell. The mixture was agitated by the electromagnetic stirrer for 10 min at stable RPM to produce CO_2 emulsion. The morphology of the CO_2 emulsion was observed through the sight window and the stability of emulsion was recorded as a function of time. In consideration of the influence of temperature and pressure on emulsion stability, the formation and stabilization experiments of CO_2 emulsions were carried out at 10–20 MPa and 25–50 °C.

2.3. Mobility evaluation and apparent viscosity measurement

The schematic of the experimental device for measuring the emulsion viscosity and resistance factor is presented in Fig. 2. This

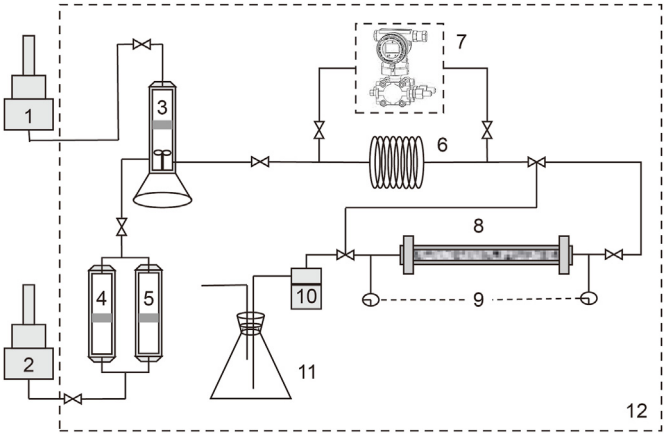

Fig. 2. Schematic diagram of mobility evaluation and apparent viscosity measurement of CO_2/H_2O emulsion.

experiment referenced the method of Chen (Chen et al., 2014) and Adkins (Adkins et al., 2010). CO_2 emulsion was prepared in the high-pressure stirred cell. An incubator and a back-pressure regulator were used to maintain the pre-set temperature and required pressure. The capillary tube was coiled, and the length and inner diameter were 1.95 m and 0.59 mm, respectively. The sand pack was filled with 100–300 mesh quartz sand, and the inner diameter and length were 18 mm and 180 mm, respectively. The porosity of the sand pack was measured with constant flow water after vacuumizing, and the permeability was confirmed by means of constant water flow according to Darcy's law. The results indicated that the sand pack in the experiments had an average porosity of 38.5% and a permeability of 201 mD. The ISCO pumps were adopted to inject fluids (CO_2/H_2O emulsion and distilled water) at constant pressure or velocity through intermediate accumulators, and the fluids flowed through the capillary tube and the sand pack in sequence. The sand pack was displaced using distilled water and the pressure was set to the target value firstly. Then the CO_2 emulsion was injected to flow through the capillary tube or the sand pack at constant velocity by regulating valves. The pressure drops across the capillary tube and the sand pack were confirmed by the differential pressure gauge and the pressure sensor.

Pressure sensors were mounted at both ends of the sand pack to monitor the inlet and outlet pressure. The resistance factor (F_R) was calculated with Eq. (1), where ΔP_w is the differential pressure for surfactant solution injection and ΔP_e is the differential pressure for emulsion flowing through the sand pack at a constant velocity.

$$F_R = \frac{\Delta P_e}{\Delta P_w} \tag{1}$$

$$\mu = \frac{\tau}{\gamma} = \frac{R_{cap}^2 \Delta P_{cap}}{8 L_c U} \tag{2}$$

The apparent viscosity of CO_2 emulsion was calculated according to the Hagen–Poiseuille equation shown in Eq. (2). In this equation: the differential pressure (ΔP_{cap}) across capillary tube was determined by the differential-pressure meter; the average velocity u was obtained from the reading of ISCO pump; and R_{cap} and L_c are the inner radius and length of the capillary tube.

2.4. Determination of physical parameters of the CO_2/H_2O emulsion and crude oil

To get sufficient knowledge about the properties of crude oil Ma 18, the component of Ma 18 was characterized by a chromatography (Agilent 7890 A). The density and viscosity of Ma 18 were confirmed by a densitometer (Anton Paar DMA4500) and viscometer (Anton Paar SVM3000) at different temperatures, respectively. In addition, the CO_2/H_2O emulsion was transferred to an Anton Paar HTHP densitometer and the density was determined at 50 °C.

2.5. Flooding experiments in a long sand pack

The schematic of the apparatus for flooding experiments in a long sand pack is presented in Fig. 3. ISCO pumps, a stirring cell and intermediate containers comprised the injection part. CO_2, brine, and surfactant solution were held in the intermediate containers, and CO_2/H_2O emulsion was prepared in the stirring tank. ISCO pumps were used to inject the aforesaid liquids. Measurements showed that the long sand pack (a 130-cm long tube with an inner diameter of 2.54 cm) used in the flooding experiments had the permeability to water of 1 D. The pressure sensors at both ends of the sand pack were used to measure the pressure gradient during the displacement. The effluent was collected and measured with a

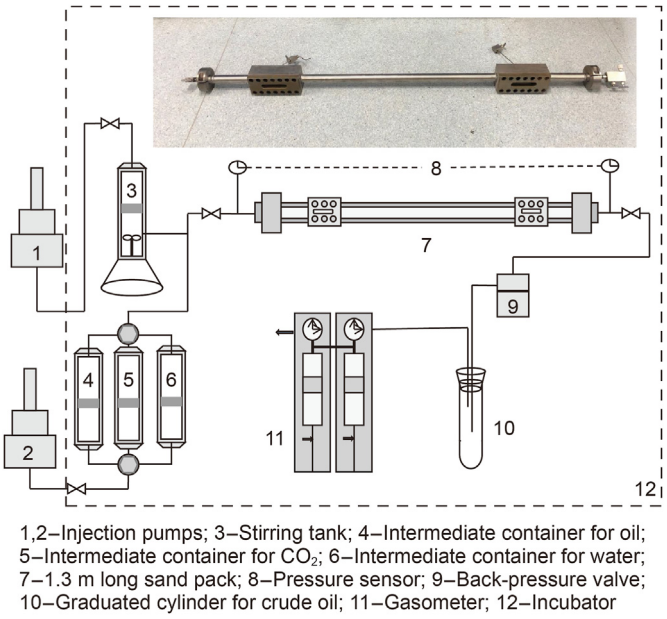

Fig. 3. Schematic diagram of the apparatus for flooding experiments in a long sand pack.

graduated cylinder and a gas meter. The back pressure valve was used to regulate the pressure of the displacement system.

The sand pack was washed with methanol and petroleum ether to ensure the impurities were moved. All apparatuses were put in an incubator and the temperature was controlled at 50 °C for 12 h. NaCl, $MgCl_2 \cdot 6H_2O$ and $CaCl_2$ were used to prepare the brine and the total salt content is 15,000 mg/L. APG was dispersed in the brine and then mixed with CO_2 under stirring, after which the CO_2 emulsion was prepared. The displacement experiments were carried out in situations without water and with water. In the experiments without initial water saturation, crude oil Ma 18 was injected directly to saturate the pore space of the sand pack tube. In the system with water saturation, the 15,000 mg/L brine was firstly injected into the sand pack to achieve sufficient brine saturation, then crude oil Ma 18 was used to displace brine until a certain water cut is reached. The detailed experimental parameters used are presented in Table 1. CO_2 flooding and CO_2/H_2O emulsion flooding were carried out, respectively, and the oil recovery and displacement curves of two displacement methods were concluded. All the flooding experiments were conducted with horizontal injection.

2.6. Core flooding experiments

The core flood apparatus is similar to the sand pack flooding apparatus and the difference is that the sand pack tube is replaced with the core holder. The core holder and core samples are shown in Fig. 4. The core holder with a length of 1.2 m is filled with three dried Berea sandstone core plugs (30 cm long and 3.8 cm in inner diameter). The core samples were saturated with brine to

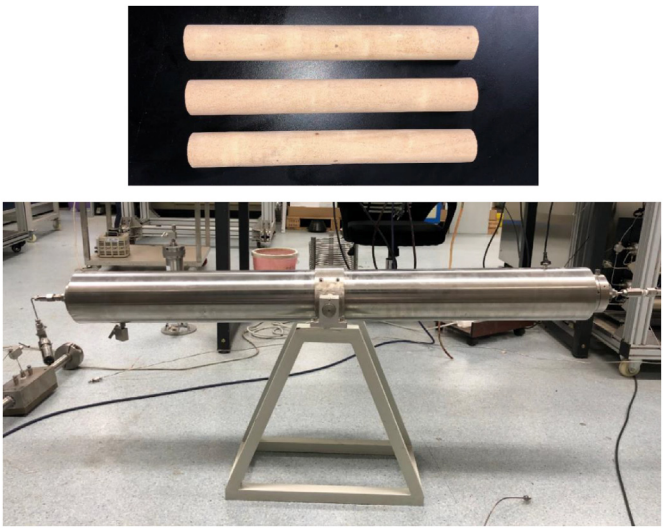

Fig. 4. The images of the core samples and the core holder.

determine pore volume after vacuumizing. One extra pump system was used to provide a confining pressure for the core samples in the core holder. Fluids including crude oil, brine, CO_2 and CO_2 emulsion (through transfer vessels) were diverted into the core sample with an ISCO pump. Pressure transducers at each end of the core holder were used to record the differential pressure across the core sample in the flooding experiments. The permeability of the core sample was determined according to the differential pressure through the core sample under constant flow rates of distilled water. The viscosity of the distilled water at standard temperature is approximately 1.0 cP and the permeability was calculated according to the Darcy formulae. 15,000 mg/L brine was firstly used to saturate the core samples after the system was vacuumed, and the crude oil Ma 18 was used to displace the brine to ensure a specific saturation with both crude oil (Ma 18) and brine. Furthermore, the pressure was increased to 12 MPa with the pump and the corresponding flooding experiments were conducted successively.

3. Results and discussion

3.1. The morphological transformation and stability of CO_2 emulsions

CO_2 emulsion is a thermodynamically unstable system. It begins phase separation under various mechanisms of destabilization such as flocculation, coalescence, sedimentation, creaming and Ostwald ripening (Torino et al., 2010). The schematic representing the emulsification and destabilization of CO_2 emulsion is shown in Fig. 5. CO_2 phase and surfactant solution phase were emulsified to a uniform CO_2 emulsion by stirring method. H_2O/CO_2 and CO_2/H_2O are two forms of emulsions which can be distinguished by different destabilization characteristics. The destabilization of H_2O/CO_2 emulsion was characterized by the turbidity reduction of emulsion

Table 1
Parameters of the flooding experiments in the long sand pack.

No.	Temperature, °C	Pressure, MPa	Saturation	Displacement
1#	50.0	19.0	Without water saturation	CO_2
2#	50.0	19.0		CO_2/H_2O emulsion
3#	50.0	19.0	With water saturation	CO_2
4#	50.0	19.0		CO_2/H_2O emulsion

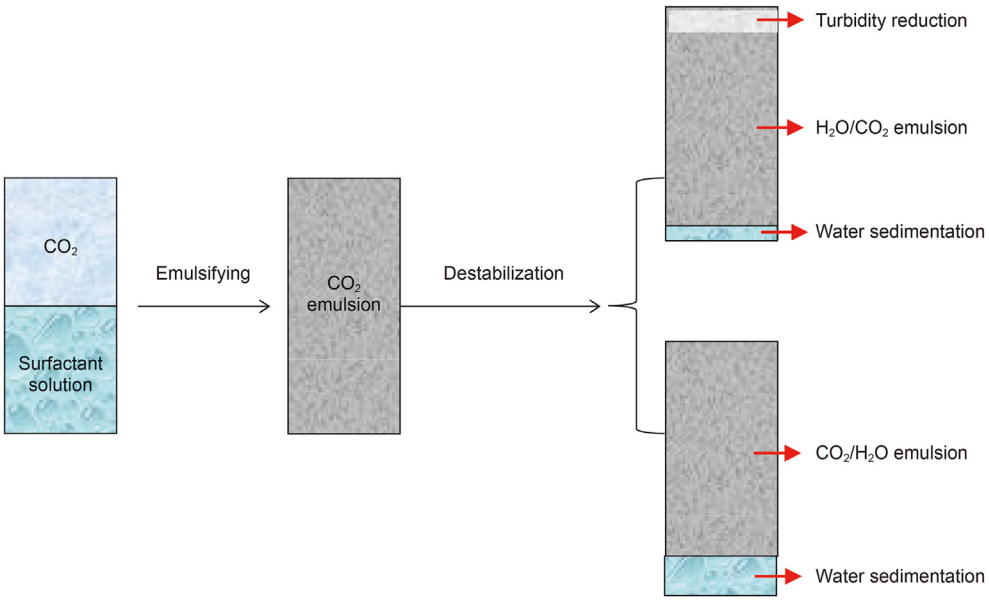

Fig. 5. The schematic diagram of emulsification and destabilization of CO_2 emulsions.

at the top of the cell. The turbidity reduction was caused by the settling of water droplets. A little of the water phase may settle because of the coalescence between dispersed water drops and gravity. However, the CO_2/H_2O emulsion showed a different destabilization feature that a clear water layer was deposited at the bottom of the cell because of the liquid film drainage. Moreover, according to Bancroft's rule, the phase which the surfactant is most likely to dissolve in is expected to become the external phase (Ruckenstein, 1996). Therefore, hydrophilic surfactants are in favor of generating the CO_2/H_2O emulsion.

Previous Qin's research suggested that CO_2 emulsion prepared with 1.5 wt% APG had a good stability, and the concentration of 1.5 wt% was much higher than the critical micelle concentration of APG (Qin et al., 2018). Thus, CO_2 emulsions were prepared with 1.5 wt% APG (refer to mass of water) in this study at 10 MPa and 25 °C. The emulsification and destabilization processes of CO_2 emulsion prepared with 16.7 vol% water cut are shown in Fig. 6. A transparent CO_2 and a surfactant solution phase were visible before stirring as shown in Fig. 6(a). After stirring for 10 min, as shown in Fig. 6(b), a milky-white emulsion occupied the whole space of the cell, suggesting that APG performed well in emulsifying. After 2.0 h, the metallic piston in the red ring was observed in Fig. 6(c), which indicated the turbidity reduction of emulsion. This turbidity reduction was resulted by the settling of water droplets, which suggested that the H_2O/CO_2 emulsion had been formed (Torino et al., 2010). The water phase caused by the settling of water droplets was not observed. This perhaps was due to a certain dead volume and too little settling water at the bottom of the PVT cell.

Also, the destabilization of CO_2/H_2O emulsions prepared with 50.0 vol% water cut is shown in Fig. 7. A milky-white CO_2 emulsion was observed in Fig. 7(a) after stirring. However, after 30 min, a transparent phase settled at the bottom of the cell, as shown in Fig. 7(b). This deposited water was caused by the quick liquid film

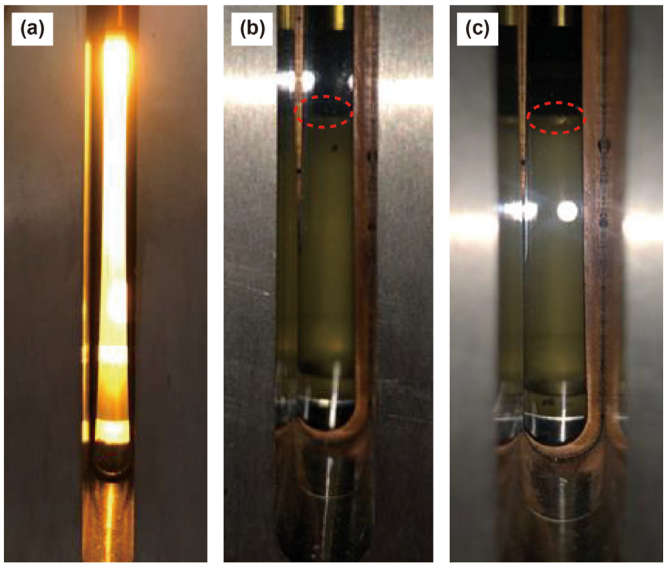

Fig. 6. Images of emulsification and destabilization of the H_2O/CO_2 emulsion (25 °C, 10 MPa, 16.7 vol% water cut).

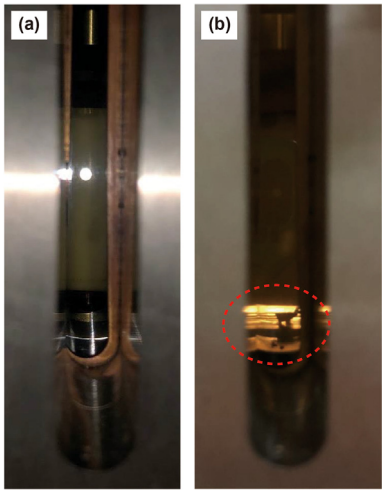

Fig. 7. Images of emulsification and destabilization of the CO_2/H_2O emulsion (25 °C, 10 MPa, 50.0 vol% water cut).

drainage rather than the settling of water droplets because the turbidity did not decrease. This suggested that the CO_2/H_2O emulsion had been formed (Torino et al., 2010). Dickson et al. also found analogous phenomenon in CO_2/H_2O emulsion (Dickson et al., 2004). In addition to the phenomenon observed, the formation of CO_2/H_2O emulsion can also be inferred because APG is more soluble in water.

The morphology inversion of CO_2 emulsions stabilized with APG is presented in Fig. 8 as a function of water cut. Phase inversion from H_2O/CO_2 emulsion to CO_2/H_2O emulsion was observed. It occurred at the water cut between 16.7 vol% and 23.1 vol%. The similar inversion of CO_2 emulsions was observed with the increase in water cut in previous studies (Lee et al., 2015; Qin et al., 2018). Bancroft's rule defined that the phase owning better solubility to surfactant is expected to be external phase (Ruckenstein, 1996). However, under the very low water cut, the violation of Bancroft's rule happened. It may be attributed to the low viscosity of the compressed CO_2, which governs several momentum and mass transfer mechanisms in emulsion formation and stabilization (Rocha et al., 2001). In addition, the H_2O/CO_2 emulsion is favored by the entropy of dispersing the relatively small amount of water in the large CO_2 phase. Furthermore, the morphology of CO_2 emulsion may be not clear enough because of the limitation of the PVT apparatus; to obtain clear morphology profiles, more effective methods such as small-angle neutron scattering are required (Wang et al., 2022).

Generally speaking, the CO_2 emulsion with better stability has higher sweep efficiency, which increases the oil recovery during oil flooding. To characterize the stability of the CO_2 emulsion, the time at which the settling water volume increased to 50 vol% of total water was regarded as the half-life. Fig. 9 presents the change of half-time as the water cut increased. As shown, CO_2 emulsions stabilized with 1.5 wt% APG showed a stability of 4–20 h at all water cuts. The emulsion transformed from H_2O/CO_2 emulsion to CO_2/H_2O emulsion with the increase in water cut, and the half-life of emulsion decreased significantly. By further improving the water cut, the half-time of CO_2 emulsion decreased slowly, but the amount of deposited water increased at the same duration. Also, the H_2O/CO_2 emulsion showed a longer half-life than the CO_2/H_2O emulsion, which indicated that the deposition rate of the aqueous

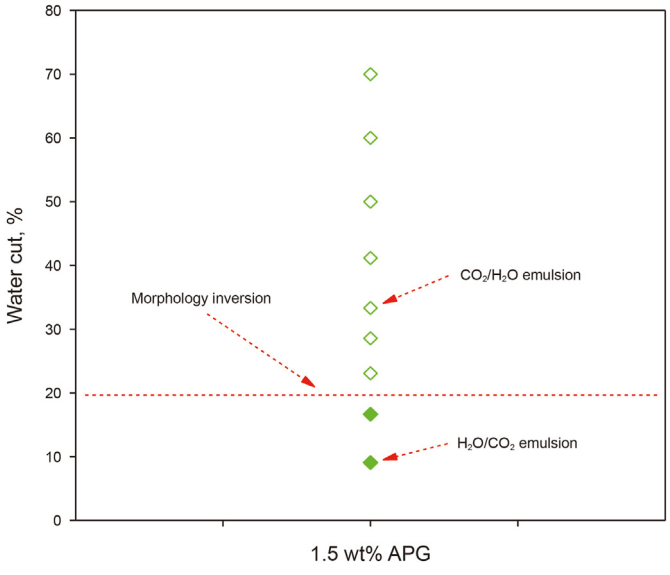

Fig. 8. Morphology inversion of CO_2 emulsions as a function of water cut (25 °C, 10 MPa).

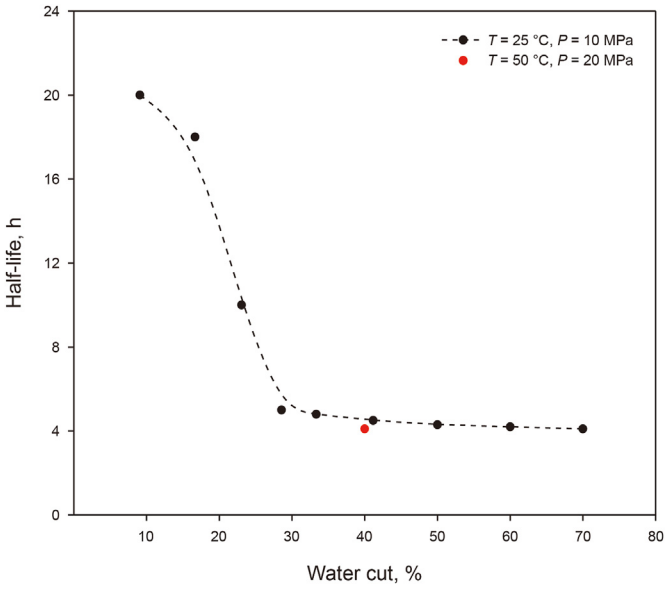

Fig. 9. Half-life of CO_2 emulsion changed with water cut.

phase as dispersion phase is significantly slower than the aqueous phase as continuous phase. Moreover, the half-life of the CO_2/H_2O emulsion, which was prepared with 40 vol% water cut at 20 MPa and 50 °C, was appended, and a mild decrease in emulsion stability was observed compared with that at 10 MPa and 25 °C. On the one hand, the decrease in CO_2 density from 817 to 784 cm^3 aggravated the liquid film drainage that arisen from gravity. On the other hand, the increased temperature accelerated the CO_2 diffusion, which weakened the liquid film strength. Both reasons may increase the deposition of water and thus decrease the half-life of the CO_2/H_2O emulsion.

3.2. Mobility reduction evaluation in sand pack and apparent viscosity measurements

As we know, the efficiency of CO_2 mobility reduction, which represents the sweep ability of emulsion in the displacement, is largely depends on emulsion apparent viscosity. Because the stability of the H_2O/CO_2 emulsion with low water cut is impaired more seriously by oil in reservoir, the CO_2/H_2O emulsion with relatively high water cut was used for the rheology investigation. The apparent viscosity of the CO_2/H_2O emulsion prepared with 1.5 wt% APG was measured by the capillary tube under a steady CO_2/H_2O emulsion flow in the tube. Fig. 10 shows the apparent viscosities of CO_2/H_2O emulsion decreased with the increase in flow velocity at all water cuts. The apparent viscosity decreased from 21.69 to 14.69 mPa s when the flow velocity of emulsion was increased from 0.5 to 2.0 mL/min at 30.0 vol% water cut. It displayed the character of non-Newtonian fluid, which characterized by the shear thinning behavior (Song et al., 2022) of the CO_2/H_2O emulsions. However, other things being equal, it decreased from 8.45 to 6.79 mPa s at 40 vol% water cut, which indicated the weakened shear thinning behavior at higher water cut. Usually, the larger the apparent viscosity value is, the better plugging performance the CO_2/H_2O emulsion gets.

To confirm the appropriate water cut of CO_2/H_2O emulsion for displacement process, the apparent viscosities at different water cuts were investigated at 25 and 50 °C. 1.0 mL/min flow velocity was adopted because the descent of apparent viscosity was small with the further increase in flow velocity. The results at 1.0 mL/min

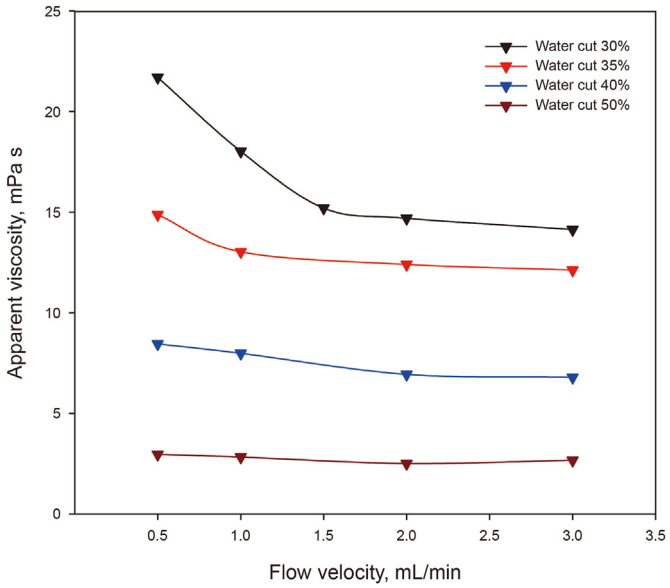

Fig. 10. Apparent viscosity of CO_2/H_2O emulsion versus flow velocity (25 °C, 20 MPa).

are presented in Fig. 11. It indicated that the water cut increased from 30 to 50 vol% caused the apparent viscosity to decrease from 18.02 to 2.83 mPa s. The decreased apparent viscosity may attribute to the emulsion texture variation with the decreased water cut (increased CO_2 fraction). Assuming a constant CO_2 droplet size in the CO_2/H_2O emulsion, the increase in water cut would decrease the lamella density, which weakens the flow resistance and decreases apparent viscosity of CO_2/H_2O emulsion (Yu and Kanj, 2022). Furthermore, the emulsion at the water cut approximately lower than 20 vol% showed different behavior (Ahmed et al., 2017a). The apparent viscosity decreased dramatically with the further decrease in water cut because the emulsion with excessively low water cut will aggravate lamellas to rupture and bubbles to coalesce. Also, the apparent viscosity of the CO_2/H_2O emulsion as a function of water cut showed a similar trend at 50 °C. However, the temperature increase produced detrimental effects on apparent viscosity of emulsion. It could be attributed to the reduced viscosity in the continuous phase. Moreover, the decreased density of CO_2 resulted from increasing temperature weakened the dissolving capacity of CO_2 to surfactant tail, which would accelerate film drainage (Chen et al., 2016).

Fig. 12 shows the apparent viscosity curve changed with pressure at 50 °C when the water cut was maintained at 40 and 50 vol%. There was a clear trend of increase in apparent viscosity with the increase in pressure at both water cuts. At water cut of 40 vol%, the apparent viscosity increased from 3.23 to 4.58 mPa s when the pressure was increased from 4 to 6 MPa, which was more remarkable than that (from 5.12 to 5.54 mPa s) when the pressure was increased from 14 to 20 MPa. A possible explanation for this might be that the elevated pressure causes the increase in CO_2 density, especially at the low pressure, thus the relative density between CO_2 and water decreased, which improved the stability of the CO_2/H_2O emulsion significantly. In addition, at higher pressure, the CO_2/H_2O emulsion formed with smaller bubble size and more uniform texture, which showed the feature of robust lamella. Both improved stability and robust lamella increase the apparent viscosity of the CO_2/H_2O emulsion. Moreover, the emulsion with 40 vol% water cut had the apparent viscosity over two time that of the emulsion with 50 vol% water cut. Combined with above research results, this implied that the CO_2/H_2O emulsions with lower water cuts (in a certain range) may have better performance during the flooding application (Li et al., 2019).

The CO_2/H_2O emulsion can reduce the CO_2 mobility by increasing the apparent viscosity and decreasing the relative permeability (Song et al., 2022). Although the apparent viscosity of the CO_2/H_2O emulsion had been evaluated by the capillary tube, it couldn't precisely reflect the rheological properties of emulsion in porous media. Therefore, the resistance factor (RF) of the CO_2/H_2O emulsion in porous media was investigated at different water cuts and temperatures through sand pack flooding experiments. In these experiments, the sand pack had the average porosity of 38.5% and the permeability of 201 mD. The resistance factor as a dimensionless value was used to evaluate the efficiency of CO_2 mobility control using the CO_2/H_2O emulsion. The greater value of the resistance factor indicated a better CO_2 mobility control efficiency. Fig. 13 presents the resistance factor values of CO_2/H_2O

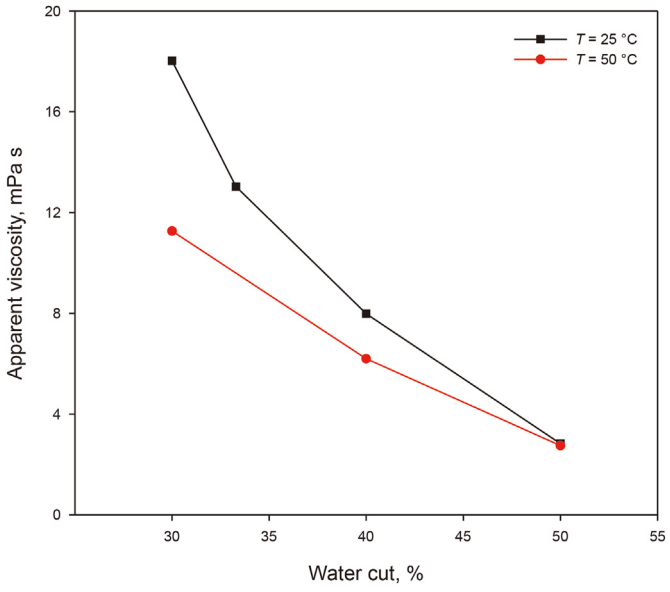

Fig. 11. Apparent viscosity curves of CO_2/H_2O emulsion with water cut (20 MPa).

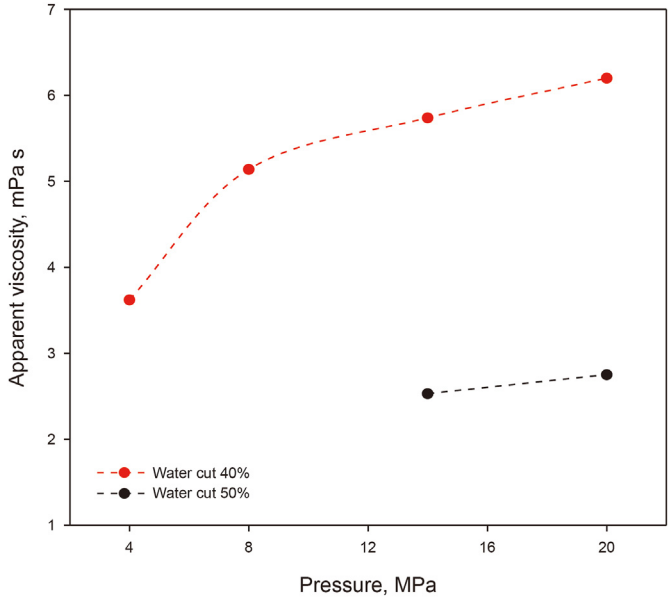

Fig. 12. Apparent viscosity curves of CO_2/H_2O emulsion at different pressure (50 °C).

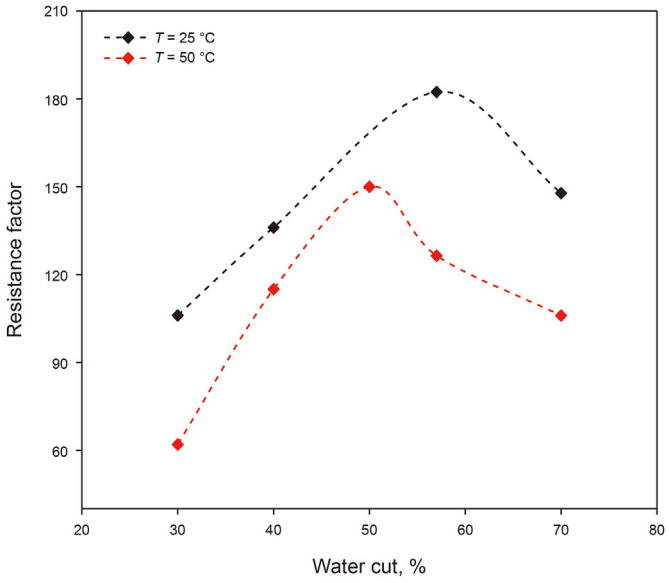

Fig. 13. Resistance factor of CO_2/H_2O emulsion changed with water cut (20 MPa).

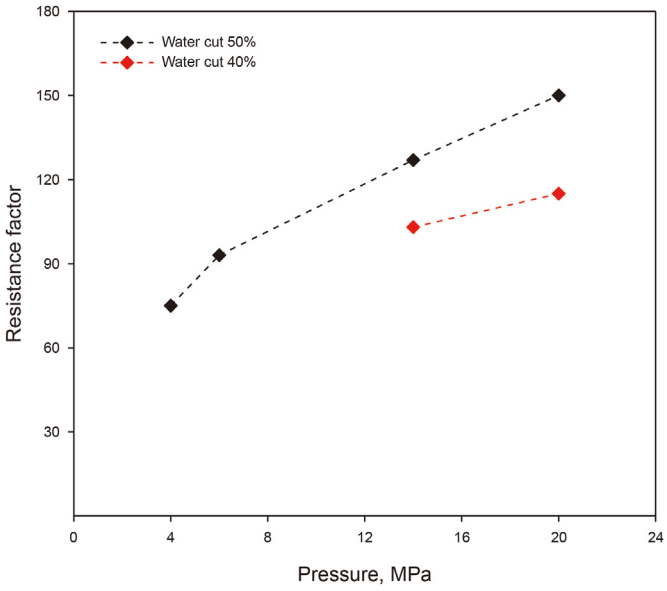

Fig. 14. Resistance factor of CO_2/H_2O emulsion versus pressure (50 °C).

emulsions as a function of water cut at 25 and 50 °C. The resistance factor increased at first and then decreased with the increase in water cut at both temperatures. The peak values of resistance factor of 182.3 and 150.0 appeared approximately at 50 and 57 vol% water cut for 25 and 50 °C, respectively. There are several possible explanations for this result. Unlike the apparent viscosity of CO_2/H_2O emulsion in the capillary tube, the resistance factor in the sand pack may be affected by more complicated parameters. Specifically, CO_2 mobility reduction represented by resistance factor in porous media is dependent on the stability and strength of the CO_2/H_2O emulsion (Abdelgawad et al., 2022). A better stability indicates a higher strength lamellae of emulsion, yet a high strength implies the finer texture emulsion consisting of smaller bubbles and more lamellae. That is to say, the flow of a fine textured emulsion may produce a higher pressure gradient, which indicates the higher flow resistance and lower CO_2 mobility (higher resistance factor) (Zhang et al., 2019b). Meanwhile, the natures of porous media such as pore size and permeability control the lamellae demolition and regeneration, and thus control the texture of the CO_2/H_2O emulsion (Lv et al., 2020). In other words, the resistance factor has a direct correlation with the permeability of porous media. In addition, the relationship between resistance factor and water cut is closely linked to permeability, and the peak of resistance factor may move to higher water cut with the increase in permeability of porous media (Jones et al., 2022). Moreover, when emulsion flows in porous media, CO_2 mobility reduction is caused by the trapped CO_2 in pores through plugging the pathway of CO_2 (Abdelgawad et al., 2022). This performance of CO_2 mobility reduction is due to the common effects of various factors such as stability, texture, permeability, trapped CO_2. The synergistic effect of these factors reached optimal result at a certain water cut which resulted in peak resistance factor. Similarly, the resistance factor of the CO_2/H_2O emulsion at 50 °C was lower than that at 25 °C. It was because the increase in temperature accelerated the bubble collapse, which was detrimental to the stability of the CO_2/H_2O emulsion.

Meanwhile, resistance factor curves as a function of pressure at water cuts of 40 and 50 vol% are shown in Fig. 14. The resistance factor of the CO_2/H_2O emulsion increased with the increase in pressure at both water cuts. At 50 vol% water cut, the resistance factor displayed more increase with pressure increase at low pressure. The stability of the CO_2/H_2O emulsion was improved with the increase in pressure, which would produce a lager flow resistance and increase the resistance factor (Wang et al., 2017). The more remarkable improvement of strength and stability of emulsion at lower pressure was due to the larger increase in resistance factor (Song et al., 2022). Moreover, the emulsion with 40 vol% water cut generated a slightly lower resistance factor at the same pressure. However, as shown in the previous result, the emulsion with 40 vol% water cut showed much larger apparent viscosity compared with that of the emulsion with 50 vol% water cut. By a comprehensive consideration, 40 vol% water cut of the CO_2/H_2O emulsion may be more appropriate for the use in flooding experiments.

3.3. *Displacement characteristics and efficiency of CO_2/H_2O emulsion in the long sand pack*

The densities of CO_2, surfactant solution and CO_2/H_2O emulsion with 1.5 wt% APG and 40 vol% water cut were measured respectively with a HTHP densimeter (Anton Paar) at different pressure and 50 °C. The results are shown in Fig. 15. It indicated that the density curve of the CO_2/H_2O emulsion was in between that of CO_2 and surfactant aqueous solution, and the densities of both CO_2 and CO_2/H_2O emulsion rose with the increase in pressure. Moreover, the density of the CO_2/H_2O emulsion was obviously higher than the density of CO_2, and the densities of CO_2 and CO_2/H_2O emulsion were 0.78 and 0.88 g/cm^3 at 20 MPa, respectively. The higher density of the CO_2/H_2O emulsion compared to CO_2 could reduce or even eliminate the influence of gravity segregation on enhancing oil recovery (Moortgat et al., 2013).

The viscosity and density of crude oil Ma18 were measured at different temperatures and the results are displayed in Fig. 16. The density and the viscosity of crude oil Ma 18 were 0.814 g/cm^3 and 6.18 mPa s at 20 °C, respectively. The density decreased linearly and the viscosity decreased exponentially with increasing temperature.

In addition, the detailed properties of crude oil Ma 18 such as API gravity, components are presented in Tables 2 and 3. The majority of components were concentrated on middle components with relatively low molecular weight (C_7–C_{18}). Meanwhile, crude oil Ma 18 showed the 41.5° of API gravity, which was regarded as a

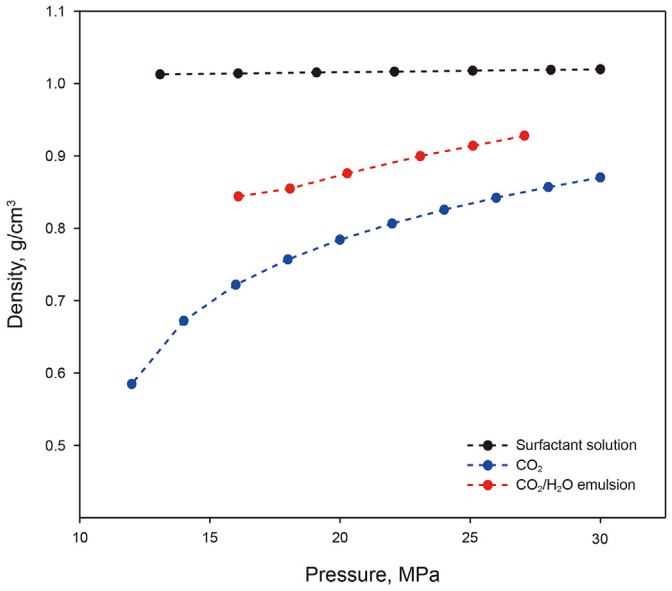

Fig. 15. Density curves of surfactant solution, CO_2 and CO_2/H_2O emulsion (50 °C).

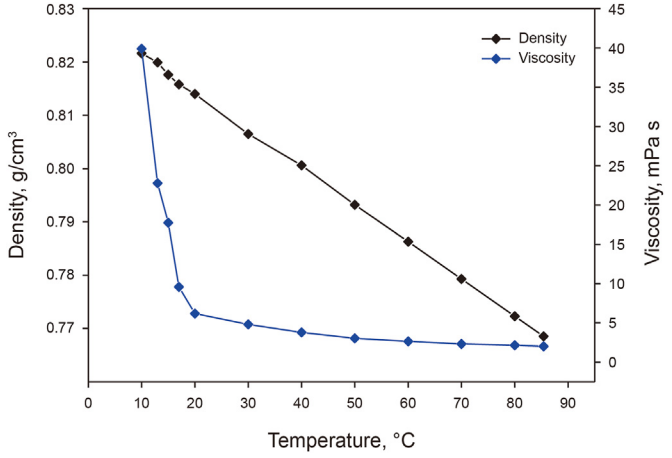

Fig. 16. Density and viscosity curves of crude oil Ma18 at the atmospheric pressure.

Table 2
Physical properties of crude oil Ma 18.

Temperature, °C	Density, kg/cm^3	Viscosity, mPa s	API gravity
20	0.814	6.176	41.5
50	0.793	3.027	

light oil.

According to the above results and taking emulsion stability, apparent viscosity and resistance factor into account, 40 vol% water cut and 1.5 wt% APG were used to prepare CO_2/H_2O emulsion for sand pack flooding experiments. The long sand pack filled with quartz sand was used to simulate the porous condition of crude oil reservoir. Flooding experiments of both CO_2 and CO_2/H_2O emulsion were conducted in the absence of water at 50 °C and 19 MPa. The injection rate was 1.0 mL/min in all the flooding experiments. Fig. 17 presents the accumulative oil recovery and gas–oil ratio (GOR) curves changed with injection volume. The results suggested that the oil recovery increased with the increase in injection volume. In contrast, although the similar linear growth appeared at the primary stage, the CO_2/H_2O emulsion injection showed a more prominent growth rate of oil recovery than that of CO_2 injection. Meanwhile, after displacement breakthrough, the CO_2/H_2O emulsion injection kept the same growth rate of oil recovery but the growth rate of oil recovery of CO_2 injection decreased significantly. Because both displacements were conducted at the same porous media, these differences of accumulative oil recovery may imply that the CO_2/H_2O emulsion displacement swept more area during the flooding. It was perhaps because the emulsion bubbles were trapped in big pores and consequently flowed to small pores because of the decreased CO_2 mobility of emulsion (Almajid and Kovscek, 2019). In addition, the growth rate of oil recovery of CO_2/H_2O emulsion injection mitigated after 1.0 PV of emulsion was injected, while this volume for CO_2 flooding was 1.2 PV. The earlier mitigation further indicated that the CO_2/H_2O emulsion flooding

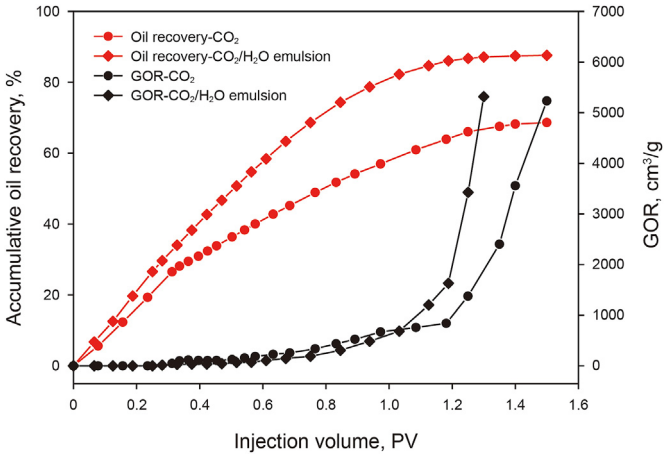

Fig. 17. Oil recovery and GOR curves of CO_2 and CO_2/H_2O emulsion flooding in the long sand pack (19 MPa, 50 °C).

Table 3
Composition of crude oil Ma 18.

Component	Mass fraction, %	Component	Mass fraction, %	Component	Mass fraction, %	Component	Mass fraction, %
< C_5	1.05	C_{13}	4.69	C_{22}	2.21	C_{31}	1.26
C_5	0.91	C_{14}	4.46	C_{23}	2.10	C_{32}	1.14
C_6	2.72	C_{15}	3.47	C_{24}	1.94	C_{33}	1.12
C_7	4.33	C_{16}	4.35	C_{25}	1.93	C_{34}	1.12
C_8	5.24	C_{17}	3.62	C_{26}	1.92	C_{35}	1.27
C_9	5.40	C_{18}	3.17	C_{27}	1.91	C_{36}	10.45
C_{10}	5.11	C_{19}	2.91	C_{28}	1.73		
C_{11}	4.53	C_{20}	2.50	C_{29}	1.64		
C_{12}	5.99	C_{21}	2.45	C_{30}	1.36		

had a better sweeping efficiency. The ultimate oil recovery of CO_2/H_2O emulsion injection was 87.63%, which was much greater than the ultimate oil recovery of pure CO_2 injection (68.65%). Therefore, the growing recovery could be attributed to the higher density and apparent viscosity of the CO_2/H_2O emulsion, which mitigated the density differential and CO_2 mobility and consequently improved the sweep efficiency. Moreover, the interfacial tension between the displacement phase and the displaced phase could be reduced effectively as existence of CO_2/H_2O emulsions, which helped to enhance the oil recovery (Chen et al., 2018).

Components of crude oils collected at different displacement stages were analyzed with a 7890A gas chromatograph. Corresponding results are shown in Fig. 18. It showed the explicit extraction of light component during both CO_2 and CO_2/H_2O emulsion flooding (Zick, 1986). An increase proportion of C_7 to C_{12} in the produced oil was observed at 0.6 PV during the injection of CO_2, but no analogous increase was observed at 0.6 PV during CO_2/H_2O emulsion injection. This indicated that, compared with the injection of CO_2/H_2O emulsion, the CO_2 injection could produce earlier effective interaction between crude oil and CO_2. This result may be explained by that the lamellae between CO_2 droplets and oil prevented the interaction between crude oil and CO_2 during CO_2/H_2O emulsion injection. As the injection volume increased, the further increase in the proportion of C_7 to C_{12} in the produced oil during CO_2 injection showed a more significant light component extraction of CO_2 at 1.0 PV and 1.5 PV during both CO_2 and CO_2/H_2O emulsion injections. Moreover, a remarkable increase in the proportion of C_8 to C_{16} was observed at 1.5 PV, indicating a significant light component extraction during CO_2/H_2O emulsion injection.

To investigate the influence of the formation water on displacement characteristics, flooding experiments of both CO_2 and CO_2/H_2O emulsion were conducted, and the sand back was saturated with water before the saturating of crude oil. Before injection, the sand pack was saturated with brine firstly, then crude oil Ma 18 was injected into the sand pack until a certain water cut was reached. The water saturations were 15.6% and 12.5% during the CO_2 flooding and CO_2/H_2O emulsion flooding, respectively. Three phases composed of brine, crude oil and displacement agent (CO_2 or CO_2/H_2O emulsion) - flowed in the sand pack during both CO_2 flooding and CO_2/H_2O emulsion flooding. The accumulative oil recovery curves and the pressure gradient curves versus injection volume are shown in Fig. 19. Initially, the accumulative oil recovery increased slowly in both the CO_2 injection and CO_2/H_2O emulsion injection. Whereas, the growth rate of oil recovery of CO_2/H_2O emulsion injection increased noticeably at 0.06 PV, and it happened at 0.2 PV during CO_2 injection. It suggested a better sweeping efficiency of CO_2/H_2O emulsion injection. Noteworthy, both CO_2 and CO_2/H_2O emulsion injection almost attained the maximum performance at 1.0 PV. The possible explanation was that the involvement of formation water may partly reduce CO_2 mobility and increase the sweeping volume of CO_2 injection (Carpenter, 2019). The improved ultimate oil recovery of CO_2 injection with the initial saturated water further confirmed the explanation. However, the formation water effect on CO_2/H_2O emulsion injection may be negligible. Finally, the total oil recovery of CO_2/H_2O emulsion injection was 87.23%, which was 15.52% higher than that of CO_2 injection. This also suggested that the better sweeping efficiency had been produced by CO_2/H_2O emulsion despite the formation water effect. The differential pressure curves showed a similar characteristic in both CO_2 flooding and CO_2/H_2O emulsion flooding. It increased with injection volume at the beginning and peaked around 0.2 PV, then decreased remarkably. However, the CO_2/H_2O emulsion injection produced higher differential pressure than CO_2 injection. This result further supported that CO_2/H_2O emulsion effectively reduced CO_2 mobility, which improved the displacement effect.

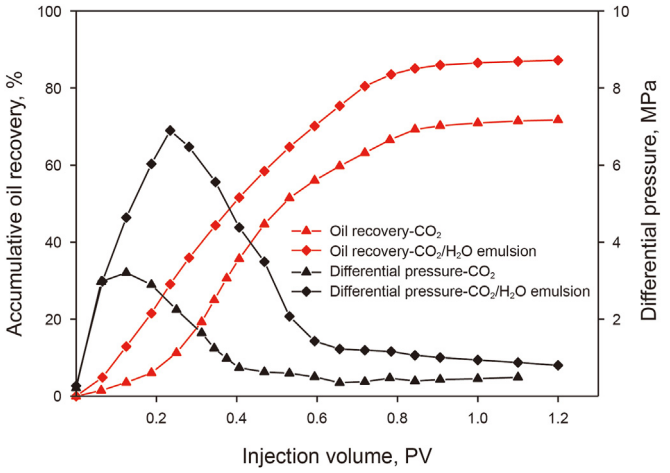

Fig. 19. Oil recovery and differential pressure curves of CO_2 and CO_2/H_2O emulsion flooding in the long sand pack (19 MPa, 50 °C).

Fig. 20 presents the produced oils at different displacement

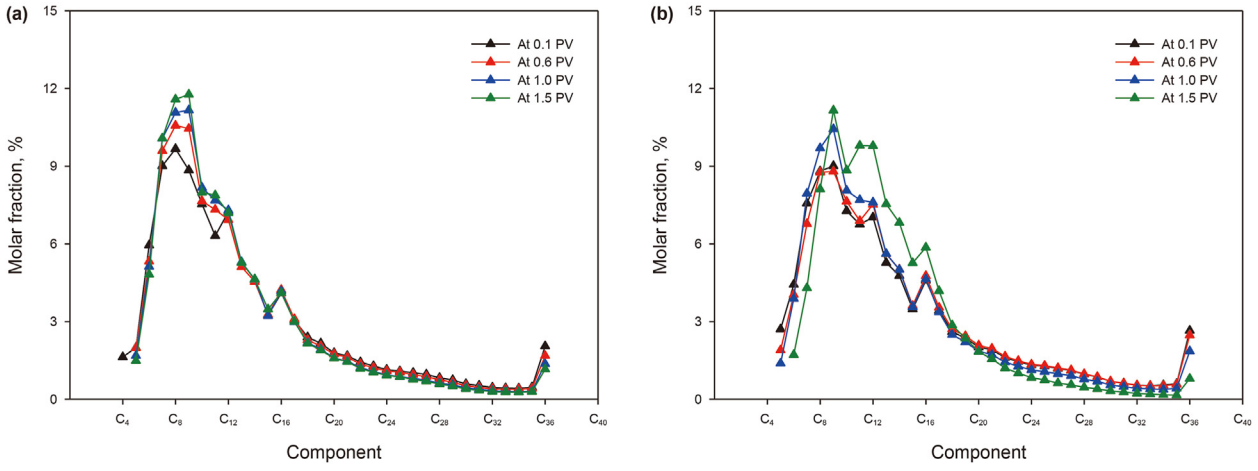

Fig. 18. Oil components of CO_2 flooding (**a**) and CO_2/H_2O emulsion flooding (**b**) at different flooding periods (19 MPa, 50 °C).

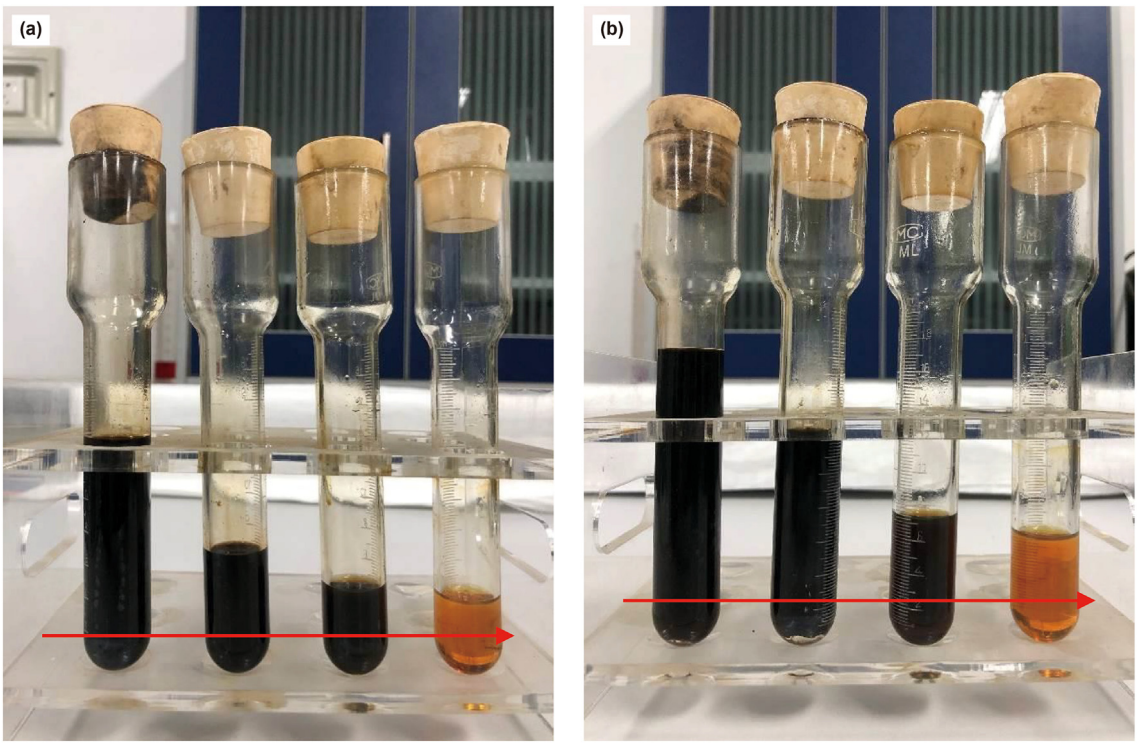

Fig. 20. Produced oil at different stages in the long sand pack displacement. (**a**) CO_2 injection; (**b**) CO_2/H_2O emulsion injection.

stages after displacing phase breakthrough. Red arrows refer to the sequence of produced oil. The produced oil got light remarkably at the final stage of the displacement. It suggested the strong miscibility of CO_2 and crude oil. Moreover, both explicit extraction and lighting of produced oil implied that miscible or near-miscible pressure was satisfied during the long sand pack flooding at 19 MPa and 50 °C. However, our previous research indicated that the CO_2/H_2O emulsion injection had better ability in improving oil recovery at immiscible displacement (Wu et al., 2020). Therefore, the displacement pressure in long core flooding was decreased to 12 MPa to ensure the immiscible displacement.

3.4. Oil recovery with different injection scenarios in core flooding

The crude oil and CO_2/H_2O emulsion used in the sand pack displacement tests were applied to the core flooding tests. The pressure of back-pressure valve was set to 12.0 MPa and the temperature was maintained at 50 °C. The experimental scenarios and parameters are showed in Table 4.

The properties of the core samples are closer to that of the oil reservoir, thus the long core flooding experiments were carried out. Fig. 21 reveals the accumulative oil recovery in different scenarios for the same core samples according to the order of injection. The different scenarios were conducted to confirm the flooding efficiency of CO_2/H_2O emulsion injection and CO_2 injection. The core samples were firstly flooded with brine in all three scenarios. It

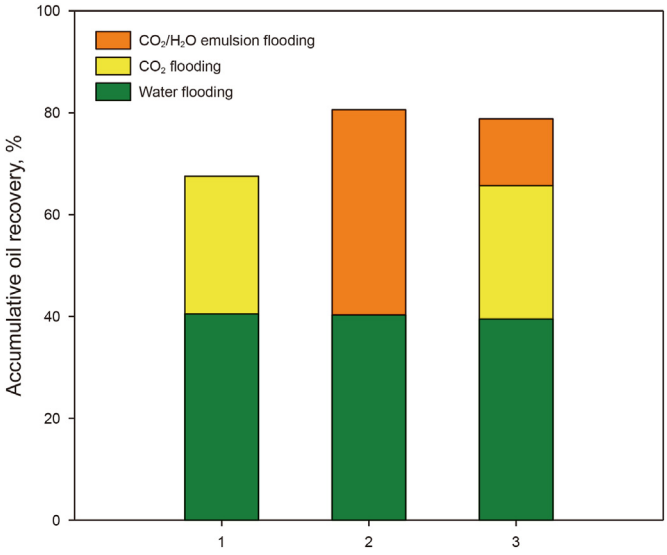

Fig. 21. Accumulative oil recovery in different injection scenarios (12 MPa, 50 °C).

suggested that the recoveries of water injection for different scenarios were all around 40.0%, which was attributed to the same physical properties of core samples. With following injections of

Table 4
Parameters of the core flooding experiments.

No.	Pressure, MPa	Temperature, °C	Injection volume of water, PV	Injection volume of CO_2, PV	Injection volume of CO_2/H_2O emulsion, PV
1	12	50	1.10	1.40	–
2	12	50	1.10	–	1.40
3	12	50	1.10	1.40	1.25

CO_2 and CO_2/H_2O emulsion, oil recovery was improved further. The accumulative oil recovery by CO_2/H_2O emulsion injection and CO_2 injection were 80.89% and 67.53%, respectively. It indicated that both CO_2 and CO_2/H_2O emulsion could be used to effectively displace the residual oil after water flooding because of the interaction of CO_2 and oil (Tan et al., 2022), but the injection of CO_2/H_2O emulsion produced 13.36% additional oil recovery. It may be attribute to that CO_2/H_2O emulsion provides an effective control on CO_2 mobility, which improved the sweep efficiency. Noteworthy, the CO_2/H_2O emulsion injection after CO_2 injection also produced an increase of 11.26% of oil recovery in the scenario 3.

In recent years, a great number of studies against the application of CO_2 emulsion in petroleum industry have been carried out. Accordingly, performances such as stability, CO_2 mobility reduction, and oil recovery enhancement by CO_2 emulsion have been evaluated by using various surface active materials (Abdelgawad et al., 2022; Burrows et al., 2022; Yu and Kanj, 2022). Meanwhile, surfactants such as olefin sulfonate, protonated ethoxylated amines, alkyl ethxoylate and betaine have shown the ability to stabilize CO_2 emulsion, and many nanoparticles also have attracted research interest (Burrows et al., 2022; Da et al., 2018; Jian et al., 2021; Song et al., 2022). Oil flooding experiments with different scenarios all suggested that more than 10% of ultimate oil recovery can be enhanced with CO_2 emulsion compared with pure CO_2 (Al Yousef et al., 2020; Jian et al., 2021). However, there are still many shortcomings and problems for pilot application off CO_2 emulsion in oil reservoir. Besides the damage of severe reservoir condition on CO_2 emulsion stability, the economy and biodegradability of formulations also need to be highlighted (Jones et al., 2022). Despite many new formulations for CO_2 emulsion preparation have shown good performance in CO_2 emulsion stability and CO_2 mobility reduction, the complicated synthetic method and high cost limit their large scale use in oil reservoirs. In this study, the nonionic surfactant APG was used and the considerable oil recovery increase was obtained. In addition, its low price and good biodegradability can ensure the large scale application. Furthermore, in consideration of the resource scarcity of natural CO_2 in China, the CO_2/H_2O emulsion flooding with 40 vol% water cut will decrease the assumption of CO_2 and the cost of flooding, which may accelerate the application of CO_2 flooding in oil production.

4. Conclusions

The CO_2 emulsion prepared with 1.5 wt% APG was evaluated. APG showed a good performance of emulsification and the corresponding CO_2 emulsion had an excellent stability. Also, an inversion of CO_2 emulsion from H_2O/CO_2 emulsion to CO_2/H_2O emulsion with the increase in water cut was confirmed. Accordingly, 1.5 wt% APG was selected to prepare CO_2/H_2O emulsions for evaluation of CO_2 mobility control and the measurement of apparent viscosity. The apparent viscosity was measured at both 25 and 50 °C, and the results suggested that the apparent viscosity decreased as the water cut increased. However, resistance factor measurement results of CO_2/H_2O emulsion indicated that the optimum performance was obtained with around 50 vol% water at both 25 and 50 °C. This result provided a reference for preparation of CO_2/H_2O emulsion in subsequent flooding experiments. In addition, a high water cut (40 vol%) was used to prepare CO_2/H_2O emulsion for flooding experiments in both long sand pack and core. The long sand pack with the permeability of 1000 mD was used to simulate the high-permeability reservoir condition and the Berea cores with an average permeability of 24.6 mD were used to simulate the low-permeability reservoir condition. The CO_2/H_2O emulsion flooding produced 18.89% and 15.52% additional oil recovery in both the absence and presence of the initial water saturation, respectively. Similarly, the additional oil recovery by injection of CO_2/H_2O emulsion was 13.0% higher than that by CO_2 injection for the cores after water flooding. Moreover, the CO_2/H_2O emulsion displacement with 40 vol% water cut would provide a more economical choice for enhancing oil recovery.

Declaration of interests

The authors declare that they have no known competing financial interests or personal relationships that could have appeared to influence the work reported in this paper.

CRediT authorship contribution statement

Xi-Dao Wu: Investigation, Writing – original draft, Formal analysis. **Peng Xiao:** Writing – review & editing, Methodology. **Bei Liu:** Conceptualization, Funding acquisition, Supervision. **Guang-Jin Chen:** Supervision. **Jian-Hua Pang:** Supervision.

Acknowledgements

The financial supports received from the National Natural Science Foundation of China (Nos. 22178378, 22127812) are gratefully acknowledged.

References

Abdelgawad, K.Z., Adebayo, A.R., Isah, A., Muhammed, N.S., 2022. A literature review of strength and stability of foam and their relationship with the absolute permeability of porous media. J. Petrol. Sci. Eng. 211, 110195. https://doi.org/10.1016/j.petrol.2022.110195.

Adkins, S.S., Chen, X., Chan, I., et al., 2010. Morphology and stability of CO_2-in-water foams with nonionic hydrocarbon surfactants. Langmuir 26 (8), 5335–5348. https://doi.org/10.1021/la903663v.

Afzali, S., Rezaei, N., Zendehboudi, S., 2018. A comprehensive review on enhanced oil recovery by water alternating gas (WAG) injection. Fuel 227, 218–246. https://doi.org/10.1016/j.fuel.2018.04.015.

Ahmed, S., Elraies, K.A., Forooozesh, J., et al., 2017a. Experimental investigation of immiscible supercritical carbon dioxide foam rheology for improved oil recovery. J. Earth Sci. 28 (5), 835–841. https://doi.org/10.1007/s12583-017-0803-z.

Ahmed, S., Elraies, K.A., Tan, I.M., Hashmet, M.R., 2017b. Experimental investigation of associative polymer performance for CO_2 foam enhanced oil recovery. J. Petrol. Sci. Eng. 157, 971–979. https://doi.org/10.1016/j.petrol.2017.08.018.

Al Hinai, N.M., Myers, M.B., Dehghani, A.M., et al., 2019. Effects of oligomers dissolved in CO_2 or associated gas on IFT and miscibility pressure with a gas-light crude oil system. J. Petrol. Sci. Eng. https://doi.org/10.1016/j.petrol.2019.106210.

Al Yousef, Z.A., Almobarky, M.A., Schechter, D.S., 2020. Surfactant and a mixture of surfactant and nanoparticles to stabilize CO_2/brine foam, control gas mobility, and enhance oil recovery. J. Pet. Explor. Prod. Technol. 10 (2), 439–445. https://doi.org/10.1007/S13202-019-0695-9.

Almajid, M.M., Kovscek, A.R., 2019. Pore network investigation of trapped gas and foam generation mechanisms. Transport Porous Media 131 (1), 289–313. https://doi.org/10.1007/s11242-018-01224-4.

Almobarak, M., Wu, Z., Zhou, D., et al., 2021. A review of chemical-assisted minimum miscibility pressure reduction in CO_2 injection for enhanced oil recovery. Petroleum 7 (3), 245–253. https://doi.org/10.1016/j.petlm.2021.01.001.

Alvarenga, B.G., Goncalves, C.C.R., Perez-Gramatges, A., 2022. Stabilization of CO_2-foams in brine by reducing drainage and coarsening using alkyldimethylamine oxides as surfactants. J. Mol. Liq. 347. https://doi.org/10.1016/j.molliq.2021.118370.

Ampomah, W., Balch, R., Cather, M., et al., 2016. Evaluation of CO_2 storage mechanisms in CO_2 enhanced oil recovery sites: application to Morrow sandstone reservoir. Energy Fuels 30 (10), 8545–8555. https://doi.org/10.1021/acs.energyfuels.6b01888.

Andrianov, A., Farajzadeh, R., Nick, M.M., Talanana, M., Zitha, P., 2011. Immiscible foam for enhancing oil recovery: bulk and porous media experiments. J. Ind. Eng. Chem. 51, 2214–2226. https://doi.org/10.1021/ie201872v.

Aryana, S.A., Kovscek, A.R., 2012. Experiments and analysis of drainage displacement processes relevant to carbon dioxide injection. Phys. Rev. E - Stat. Nonlinear Soft Matter Phys. 86, 06630. https://doi.org/10.1103/physreve.86.066310.

Beheshti, E., Riahi, S., Riazi, M., 2022. Impacts of oil components on the stability of aqueous bulk CO_2 foams: An experimental study. Colloids Surf. A-Physicochem. Eng. Asp. 648. https://doi.org/10.1016/j.colsurfa.2022.129328.

Binks, B.P., Campbell, S., Mashinchi, S., Piatko, M.P., 2015. Dispersion behavior and

aqueous foams in mixtures of a vesicle-forming surfactant and edible nanoparticles. Langmuir 31 (10), 2967–2978. https://doi.org/10.1021/la504761x.
Boeije, C.S., Rossen, W.R., 2018. SAG foam flooding in carbonate rocks. J. Pet. Sci. Eng. 171, 30683–30702. https://doi.org/10.3997/2214-4609.201700337.
Burrows, L.C., Haeri, F., Tapriyal, D., et al., 2022. Dissolving nonionic surfactants in CO_2 to improve oil recovery in unconventional reservoirs via wettability alteration. Energy Fuels 36 (19), 11913–11929. https://doi.org/10.1021/acs.energyfuels.2c02203.
Carpenter, C., 2019. Experimental program investigates miscible CO_2 WAG injection in carbonate reservoirs. J. Petrol. Technol. 71 (1), 47–49. https://doi.org/10.2118/0119-0047-JPT.
Chen, Y., Elhag, A.S., Poon, B.M., et al., 2014. Switchable nonionic to cationic ethoxylated amine surfactants for CO_2 Enhanced oil recovery in high-temperature, high-salinity carbonate reservoirs. SPE J. 19 (2), 249–259. https://doi.org/10.2118/154222-PA.
Chen, Y., Elhag, A.S., Reddy, P.P., et al., 2016. Phase behavior and interfacial properties of a switchable ethoxylated amine surfactant at high temperature and effects on CO_2-in-water foams. J. Colloid Interface Sci. 470, 80–91. https://doi.org/10.1016/j.jcis.2016.02.028.
Chen, H., Elhag, A.S., Chen, Y., et al., 2018. Oil effect on CO_2 foam stabilized by a switchable amine surfactant at high temperature and high salinity. Fuel 227, 247–255. https://doi.org/10.1016/j.fuel.2018.04.020.
Da, C., Jian, G., Alzobaidi, S., et al., 2018. Design of CO_2-in-water foam stabilized with switchable amine surfactants at high temperature in high-salinity brine and effect of oil. Energy Fuels 32 (12), 12259–12267. https://doi.org/10.1021/acs.energyfuels.8b02959.
Dickson, J.L., Binks, B.P., Johnston, K.P., 2004. Stabilization of carbon dioxide-in-water emulsions with silica nanoparticles. Langmuir 20 (19), 7976–7983. https://doi.org/10.1021/la0488102.
Enick, R.M., Olsen, D.K., Ammer, J.R., Schuller, W., 2012. Mobility and conformance control for CO_2 EOR via thickeners, foams, and gels - A literature review of 40 years of research and pilot tests. In: SPE Improved Oil Recovery Symposium. https://doi.org/10.2118/154122-MS.
Fyen, T., Alcorn, Z.P., Fern, M.A., Barrabino, A., Holt, T., 2020. CO_2 mobility reduction using foam stabilized by CO_2- and water-soluble surfactants. J. Petrol. Sci. Eng. https://doi.org/10.1016/j.petrol.2020.107651.
Grassia, 2015. Foam stability in the presence and absence of hydrocarbons: from bubble- to bulk-scale. Colloids Surf. A Physicochem. Eng. Asp. 481, 512–526. https://doi.org/10.1016/J.COLSURFA.2015.06.023.
Hematpur, H., Mahmood, S.M., Nasr, N.H., et al., 2018. Foam flow in porous media: concepts, models and challenges. J. Nat. Gas Sci. Eng. https://doi.org/10.1016/j.jngse.2018.02.017.
Jian, G., Alcorn, Z., Zhang, L., Puerto, M.C., Hirasaki, G.J., 2020. Evaluation of a nonionic surfactant foam for CO_2 mobility control in a heterogeneous carbonate reservoir. SPE J. 25 (6), 1–13. https://doi.org/10.2118/203822-PA.
Jian, G., Fernandez, C.A., Puerto, M., et al., 2021. Advances and challenges in CO_2 foam technologies for enhanced oil recovery in carbonate reservoirs. J. Petrol. Sci. Eng. 202. https://doi.org/10.1016/j.petrol.2021.108447.
Jones, S.A., Kahrobaei, S., van Wageningen, N., Farajzadeh, R., 2022. CO_2 foam behavior in carbonate rock: effect of surfactant type and concentration. Ind. Eng. Chem. Res. https://doi.org/10.1021/acs.iecr.2c01186.
Kharazi, M., Saien, J., 2022. Mechanism responsible altering in interfacial tension and emulsification of the crude oil-water system with nano Gemini surface active ionic liquids, salts and pH. J. Petrol. Sci. Eng. 219. https://doi.org/10.1016/j.petrol.2022.111090.
Kharazi, M., Saien, J., Torabi, M., Zolfigol, M.A., 2023. Molecular design and applications of a nanostructure green Tripodal surface active ionic liquid in enhanced oil recovery: interfacial tension reduction, wettability alteration, and emulsification. Petrol. Sci. https://doi.org/10.1016/j.petsci.2023.07.010.
Lee, C.T., Psathas, P.A., Johnston, K.P., Degrazia, J., Randolph, T.W., 2015. Water-in-carbon dioxide emulsions: formation and stability. Langmuir 15 (20), 6781–6791. https://doi.org/10.1021/la9903548.
Li, W., Zeng, H., 2022. Effect of temperature on the stability of supercritical CO_2 foam stabilized with a betaine surfactant at high pressure. Colloids Surf. A Physicochem. Eng. Asp. 649. https://doi.org/10.1016/j.colsurfa.2022.129362.
Li, R.F., Yan, W., Liu, S., Hirasaki, G.J., Miller, C.A., 2010. Foam mobility control for surfactant enhanced oil recovery. SPE J. 15 (4), 928–942. https://doi.org/10.2118/113910-PA.
Li, Q., Chen, Z., Zhang, J., et al., 2016. Positioning and revision of CCUS technology development in China. Int. J. Greenh. Gas Control 46, 282–293. https://doi.org/10.1016/j.ijggc.2015.02.024.
Li, B., Li, H., Cao, A., Wang, F., 2019. Effect of surfactant concentration on foam texture and flow characteristics in porous media. Colloids Surf. A Physicochem. Eng. Asp. 560, 189–197. https://doi.org/10.1016/j.colsurfa.2018.10.027.
Lv, M., Liu, Z., Jia, L., Ji, C., 2020. Visualizing pore-scale foam flow in micromodels with different permeabilities. Colloids Surf. A: Physicochem. Eng. Aspects vol. 600. https://doi.org/10.1016/j.colsurfa.2020.124923.
Massarweh, O., Abushaikha, A.S., 2021. A review of recent developments in CO_2 mobility control in enhanced oil recovery. Petroleum 8 (3), 291–317. https://doi.org/10.1016/j.petlm.2021.05.002.
Mathew, E.S., Shaik, A.R., AlSumaiti, A., Alameri, W.S., 2018. Effect of oil presence on CO_2 foam based mobility control in high temperature high salinity carbonate reservoirs. Energy Fuels 32 (3), 2983–2992. https://doi.org/10.1021/acs.energyfuels.7b03490.
Moortgat, J., Firoozabadi, A., Li, Z., Esposito, R., 2013. CO_2 Injection in vertical and horizontal cores: measurements and numerical simulation. SPE J. 18 (2), 331–344. https://doi.org/10.2118/135563-PA.
Orr, F.M., Taber, J.J., 1984. Use of carbon dioxide in enhanced oil recovery. Science 224 (4649), 563–569. https://doi.org/10.1126/science.224.4649.563.
Osei-Bonsu, K., Shokri, N., Grassia, P., 2015. Fundamental investigation of foam flow in a liquid-filled Hele-Shaw cell. J. Colloid Interface Sci. 462, 288–296. https://doi.org/10.1016/j.jcis.2015.10.017.
Qin, H., Sun, X., Sun, C., et al., 2018. Applicability of nonionic surfactant alkyl polyglucoside in preparation of liquid CO_2 emulsion. J. CO_2 Util. 26, 503–510. https://doi.org/10.1016/j.jcou.2018.06.005.
Rocha, S.R., Psathas, P.A., Klein, E., Johnston, K.P., 2001. Concentrated CO_2-in-water emulsions with nonionic polymeric surfactants. J. Colloid Interface Sci. 239 (1), 241–253. https://doi.org/10.1006/jcis.2001.7544.
Rondón-González, M., Sadtler, V., Marchal, P., Choplin, L., Salager, J.L., 2008. Emulsion catastrophic inversion from abnormal to normal morphology. 7. Emulsion evolution produced by continuous stirring to generate a very high internal phase ratio emulsion. Ind. Eng. Chem. Res. 47 (7). https://doi.org/10.1021/ie071482r.
Ruckenstein, E., 1996. Microemulsions, macroemulsions, and the bancroft rule. Langmuir 12, 6351–6353. https://doi.org/10.1021/la960849m.
Safran, S.E., Kok, M.V., 2022. Nanoparticle-stabilized CO_2 foam to improve conventional CO_2 EOR process and recovery at Bati Raman oil field, Turkey. J. Petrol. Sci. Eng. 208. https://doi.org/10.1016/j.petrol.2021.109547.
Song, Z., Hou, J., Liu, X., et al., 2018. Conformance control for CO_2 -EOR in naturally fractured low permeability oil reservoirs. J. Petrol. Sci. Eng. 225–234. https://doi.org/10.1016/j.petrol.2018.03.030.
Song, Z., Li, Y., Song, Y., et al., 2020. A critical review of CO_2 enhanced oil recovery in tight oil reservoirs of North America and China. Fuel 276. https://doi.org/10.2118/196548-MS.
Song, X., Cui, X., Su, X., Munir, B., Du, D., 2022. Laboratory study on the rheology properties of nanoparticle-stabilized supercritical CO_2 foam. J. Petrol. Sci. Eng. 218. https://doi.org/10.1016/j.petrol.2022.111065.
Tan, Y., Li, Q., Xu, L., et al., 2022. A critical review of carbon dioxide enhanced oil recovery in carbonate reservoirs. Fuel 328. https://doi.org/10.1016/j.fuel.2022.125256.
Torino, E., Reverchon, E., Johnston, K.P., 2010. Carbon dioxide/water, water/carbon dioxide emulsions and double emulsions stabilized with a nonionic biocompatible surfactant. J. Colloid Interface Sci. 348 (2), 469–478. https://doi.org/10.1016/j.jcis.2010.04.027.
Waltermo, S., Claesson, P.M., Simonsson, S., Manev, E., Bergeron, V., 1996. Foam and thin-liquid-film studies of alkyl glucoside systems. Langmuir 12 (22), 5271–5278. https://doi.org/10.1021/la9601723.
Wang, Y., Zhang, Y., Liu, Y., Zhang, L., 2017. The stability study of CO_2 foams at high pressure and high temperature. J. Petrol. Sci. Eng. 30437, 1–34. https://doi.org/10.1016/j.petrol.2017.04.029.
Wang, J., Luo, X., Rogers, S., Li, P., Feng, Y., 2022. Stabilization of CO_2 aqueous foams at high temperature and high pressure: small-angle neutron scattering and rheological studies. Colloids Surf. A Physicochem. Eng. Asp. 647. https://doi.org/10.1016/j.colsurfa.2022.129015.
Wu, X., Zhang, Y., Zhang, K., Liu, B., Xiao, P., 2020. An experimental investigation of liquid CO_2-in-water emulsions for improving oil recovery. Fuel 288, 119734. https://doi.org/10.1016/j.fuel.2020.119734.
Yu, W., Kanj, M.Y., 2022. Review of foam stability in porous media: the effect of coarsening. J. Petrol. Sci. Eng. 208. https://doi.org/10.1016/j.petrol.2021.109698.
Zhang, Y., Wang, Y., Xue, F., et al., 2015. CO_2 foam flooding for improved oil recovery: reservoir simulation models and influencing factors. J. Petrol. Sci. Eng. 133, 838–850. https://doi.org/10.1016/j.petrol.2015.04.003.
Zhang, P., Bai, P., Cui, G., et al., 2019a. Enhanced CO_2 foam based on amide and amine surfactants and synergistically coupled with sodium dodecyl sulfate at high temperature and high pressure. J. Pet. Sci. Eng. 179, 266–275. https://doi.org/10.1016/j.petrol.2019.04.070.
Zhang, X., Zhang, W., Ge, T., et al., 2019b. CO_2 in water foam stabilized with CO_2-dissolved surfactant at high pressure and high temperature. J. Petrol. Sci. Eng. 178, 930–936. https://doi.org/10.1016/j.petrol.2019.03.066.
Zhang, Y., Gao, M., You, Q., et al., 2019c. Smart mobility control agent for enhanced oil recovery during CO_2 flooding in ultra-low permeability reservoirs. Fuel 241, 442–450. https://doi.org/10.1016/j.fuel.2018.12.069.
Zick, A.A., 1986. A combined condensing/vaporizing mechanism in the displacement of oil by enriched gases. SPE Annu. Tech. Conf. Exhib. https://doi.org/10.2118/15493-MS.